Block Copolymer Self-Diffusion in the Gyroid and Cylinder Morphologies

Mark W. Hamersky,[†] Marc A. Hillmyer,[‡] Matthew Tirrell,[†] Frank S. Bates,[†] and Timothy P. Lodge*,[‡]

Departments of Chemistry and of Chemical Engineering & Materials Science, University of Minnesota, Minneapolis, Minnesota 55455

Ernst D. von Meerwall

Department of Physics and Maurice Morton Institute of Polymer Science, University of Akron, Akron, Ohio 44325

Received October 7, 1997; Revised Manuscript Received May 8, 1998

ABSTRACT: Forced Rayleigh scattering (FRS) and pulsed-field-gradient NMR have been used to measure the self-diffusion coefficient, D, of a poly(ethylene oxide)−poly(ethylethylene) diblock copolymer in the molten state. The copolymer contains 42% PEO by volume and has a total molecular weight of 4100 g/mol. Upon heating from room temperature the sample transforms from crystalline lamellae to hexagonal cylinders, and then to a bicontinuous cubic "gyroid" phase (with $Ia\bar{3}d$ space group symmetry), before finally disordering at 175 °C. FRS measurements were performed in the gyroid and cylinder phases, and NMR measurements in the gyroid and disordered states. Cylinder samples both with and without shear alignment were employed. A hysteresis loop permitted measurements of D in both cylinder and gyroid phases at the same temperature (60 °C). FRS decays from cylindrical samples were described by a sum of two exponentials. For the aligned samples, values of the diffusivity along (D_{par}) and across (D_{perp}) the cylinders were extracted; the mobility along the cylinders was approximately 2 orders of magnitude larger. This is consistent with the estimated enthalpic penalty for withdrawing the minor block from the cylindrical microdomain. FRS decays from the gyroid phase were consistently single exponential and gave a diffusivity consistent with D_{par} in the cylinders, reduced by the tortuosity of the gyroid network. The FRS and NMR results agreed very well, and the mobility varied smoothly with temperature through the order−disorder transition. However, the magnitude of the copolymer mobility was significantly lower than that of either constituent homopolymer or of two other disordered PEO−PEE diblocks, even after accounting for differences in molecular weight. This is tentatively attributed to the onset of entanglement effects.

Introduction

The relationship between microstructure and dynamics continues to be an active area of research in such soft materials as liquid crystals, surfactants, and block copolymers. The physics of such problems embodies a combination of interesting phenomena. For example, self-diffusion in a microphase-separated A−B diblock copolymer melt involves at least three issues: (i) thermodynamic penalties for A/B segment contacts, which act to localize the covalent A−B junctions to the interfaces between microdomains; (ii) mechanisms of center-of-mass motion that depend on chain length and morphology; (iii) differences in the magnitude and temperature dependence of the monomeric friction factor between blocks, which may well be functions of local composition. All these issues arise in considering the anisotropy of block copolymer motion in the ordered state: how different are the diffusivities along (D_{par}) and through (D_{perp}) the interface between microdomains? Recent studies have shed considerable light on this problem.[1−11] In particular, it appears that for *unentangled* copolymers the anisotropy is rather *large* ($D_{par}/D_{perp} > 10$), due to the ability of the chains to move along the interface without mixing the two blocks,[3,4,8,9] whereas for *entangled* copolymers the anisotropy is *small*, due to a reduction of D_{par} attributed to the inability of a chain to reptate without mixing the two blocks.[2,6,7]

The previous measurements have emphasized lamellar systems, where the interface presents a two-dimensional manifold for D_{par}. In quenched lamellar samples (i.e., those with no long-range alignment of domains) the measured mobility is dominated by D_{par} and is rather insensitive to D_{perp}. In contrast, the cylindrical and body-centered-cubic sphere morphologies have interfaces that are connected in one and zero dimensions, respectively, and could provide more quantitative information about D_{perp}. Alternatively, the bicontinuous gyroid morphology presents a three-dimensionally connected interface, and the mobility may be completely independent of D_{perp}. Practical difficulties arise when varying morphology. If the two blocks differ significantly in their monomeric friction factors or entanglement molecular weights, the inevitable changes in composition, molecular weight, and temperature may lead to substantial changes in D that are not purely thermodynamic in origin. Consequently, it is desirable to change morphology with as little change in molecular structure as possible.

In this paper, we study the effects of morphology on the self-diffusion of a molten poly(ethylene oxide-*b*-ethylethylene) (PEO−PEE) block copolymer. The copolymer exhibits thermotropic transitions between crystalline lamellar (L_c), hexagonal cylinder (C), and $Ia\bar{3}d$ ("gyroid") (G) microphases, as observed by small-angle

[†] Department of Chemical Engineering & Material Science.
[‡] Department of Chemistry.

S0024-9297(97)01476-9 CCC: $15.00
Published on Web 07/23/1998

X-ray scattering and rheology.[12,13] Diffusion measurements were performed by forced Rayleigh scattering (FRS) in both quenched and shear-aligned C phases, and by FRS and pulsed-field-gradient NMR in the G microstructure. By virtue of a thermal hysteresis loop in the copolymer phase behavior, it proved possible to measure D in both C and G phases at a single temperature, thus providing an unusually direct determination of the effect of microstructure on chain mobility. The anisotropy of motion in the C phase is large, but consistent with the expected enthalpic penalty for mixing the two blocks. Diffusivity in the G phase is interpreted in terms of the mobility along a cylindrical strut combined with the tortuosity of the network structure. The results are also compared with the self-diffusivities of the constituent homopolymers and of two other disordered PEO−PEE copolymers.

Experimental Section

Synthesis and Labeling. The synthesis of the poly(ethylene oxide-*b*-ethylethylene) block copolymers and poly(ethylethylene) homopolymer used in this study was achieved through sequential living anionic polymerization and has been described elsewhere.[14] The synthetic route began with the polymerization of 1,3-butadiene in THF with *sec*-butyllithium as the initiator to form poly(1,2-butadiene), which was end-functionalized with ethylene oxide to produce a monohydroxyl-terminated polybutadiene. This material was then catalytically hydrogenated, yielding the analogous monohydoxyl-terminated poly(ethylethylene) (PEE-OH). For the diblock copolymers, the PEE-OH was converted to the corresponding potassium alkoxide, which became the initiator for the ethylene oxide polymerization. The PEO block also contains a hydroxy terminus, which provides an attachment site for labeling the chain with 4′-(*N*,*N*-dimethylamino)-2-nitrostilbene-4-carboxylic acid (ONS). This dye was synthesized as previously described.[5,8] The labeling reaction was carried out in methylene chloride at 45 °C, using a 5-fold molar excess of dye to polymer, for 2 weeks in the absence of light. Polymer recovery was accomplished by evaporating most of the solvent and then drying under high vacuum. To separate the unattached dye from the labeled polymer, the recovered mixture was passed through a silica gel column using methylene chloride as the mobile phase. Gel permeation chromatography (GPC) indicated that the molecular weight distribution had not been altered during the labeling process and UV detection confirmed that the polymer was labeled and the free dye had been removed. The labeled polymer was then vacuum-dried and stored in the dark at −15 °C.

Characterization. The complete characterization of the PEO−PEE copolymer emphasized in this study has been reported elsewhere, where it was designated OE-6.[14] Briefly, the molecular weight of the PEE-OH block, M_{PEE}, was calculated to be 2100, using the number of repeat units (as measured by ^{1}H NMR spectroscopy on the unsaturated precursor), and the molecular weight of the initiator fragment and of the hydroxy terminus. GPC was performed on the PEE-OH, indicating a polydispersity, M_w/M_n, of 1.07. The molecular weight of the PEO block, M_{PEO}, was calculated to be 2000, based on the PEE-OH initiator concentration and the mass of EO monomer added to the reaction and assuming quantitative conversion. The overall polydispersity determined by GPC was 1.09. Finally, the volume fraction of PEO, f_{PEO}, for OE-6 was calculated to be 0.42 using densities of 0.806 and 1.06 g/mL for PEE and PEO, respectively.[15] Two other PEO−PEE copolymers, OE-12 and OE-13, were also examined for comparison purposes: OE-12 has $M_n = 2200$, $f_{PEO} = 0.52$, and $M_w/M_n = 1.11$, and OE-13 has $M_n = 2500$, $f_{PEO} = 0.73$, and $M_w/M_n = 1.11$. Furthermore, OE-12 has a methyl terminus, whereas OE-13 (and OE-6) are capped by a hydroxyl group.[14] The PEE homopolymer employed in this study has a molecular weight, M_n, of 1200 with a polydispersity of 1.08.

Rheology. Dynamic mechanical measurements were performed on a Rheometrics RSA-II solids analyzer operated in oscillatory mode, using a 1-mm-thick shear sandwich geometry. Following sample insertion at room temperature, the material was heated above the PEO melting temperature (ca. 40 °C) to facilitate loading. The dynamic shear moduli, G' and G'', were then measured during isochronal temperature sweeps, at a frequency of 0.5 rad/s and a heating rate of 1 °C/min. Strain amplitudes were less than 2%, and the temperature was controlled to within 1 °C over the range 25−180 °C by a thermally regulated nitrogen gas purge within the sample chamber.

Small-Angle X-ray Scattering. X-ray scattering experiments were carried out on a SAXS instrument that utilizes Cu K_α radiation ($\lambda = 1.54$ Å) emanating from a Rigaku RU-200BVH rotating anode generator equipped with an 0.2 mm × 2 mm microfocus cathode and Franks mirror optics. Two-dimensional SAXS patterns were recorded on a Siemens multiwire area detector located at the end of a 1.0 m evacuated flight tube. Samples were placed inside an evacuated chamber and annealed for 10 min before beginning X-ray experiments. Sample temperatures were maintained to within ±0.1 °C by resistive heaters mounted in a water-cooled brass block. All SAXS data were corrected for detector response prior to analysis.

Forced Rayleigh Scattering. Diffusion coefficients were measured by FRS using the experimental apparatus and data analysis schemes described elsewhere.[16,17] A transient grating was formed in the sample by crossing two mutually coherent Ar^+ laser beams ($\lambda_o = 488$ nm). The duration of this "writing" pulse was typically 100 ms. Erasure of the grating, due to center-of-mass diffusion, was monitored by directing one of the same beams (attenuated by a factor of 10^4) to the grating location and measuring the diffracted intensity at the first-order Bragg angle. In all cases, a single-shot experiment was sufficient to provide excellent signal-to-noise. The diffracted intensity was usually well-described by the following expression:

$$I(t) = [A \exp(-t/\tau) + B]^2 + C^2 \quad (1)$$

where A denotes the amplitude, τ the decay time, and B and C the coherent and incoherent baseline contributions, respectively. In cases where the above model did not give satisfactory agreement with the data, the following double exponential expression was used:

$$I(t) = [A_1 \exp(-t/\tau_1) + A_2 \exp(-t/\tau_2)]^2 + C^2 \quad (2)$$

where A_1 and A_2 are amplitudes, τ_1 and τ_2 are decay times, and C is the incoherent background.

FRS samples were prepared as follows. Appropriate amounts of labeled (tracer, 0.8 mg) and unlabeled (matrix, 100 mg) OE-6 were codissolved in methylene chloride (4−5% g/mL). The solution was forced through an 0.45 μm nylon filter with a syringe. Most of the solvent was removed by evaporation, and then the polymer was vacuum-dried to constant weight. One specimen was heated to 185 °C under vacuum to disorder the copolymer and to allow it to flow into an FRS cell consisting of two 25 mm diameter quartz disks (Heraeus Amersil) separated by 1 mm, fused along the perimeter with quartz except for a 5 mm gap to permit filling. This sample was cooled under vacuum quiescently, which took approximately 10 h, leaving the material in a "quenched" state (i.e., ordered but not macroscopically aligned), and then sealed with epoxy under an argon atmosphere. The other sample was subjected to a shear field to create macroscopic alignment prior to FRS experiments (see below).

Samples were placed in a copper block equipped with resistive heaters to maintain temperature control to within ±0.2 °C. For each temperature studied, the sample was first equilibrated for 15 min and then the decay function was recorded for at least three values of grating spacing, d, over a range from 1 to 22 μm. For each experiment, 1000 data points

were acquired, although for clarity, only a subset are shown in plots (see Figures 3a and 5).

Shear Alignment. A reciprocating shear field was applied to the sample to establish a preferred direction of alignment. The shearing apparatus employed a pair of parallel PTFE-covered brass plates with a 1 mm gap.[18] The temperature was held at 60 °C for the duration of the shearing and controlled to ±1 °C with resistive heaters and a thermocouple located in each block. The strain amplitude was maintained at 100%, and the frequency was 1.3 rad/s for the first 1.5 h and 0.2 rad/s for a subsequent 2 h, which corresponds to approximately 1200 total shear cycles. After the shear direction was marked on the sample, it was removed from the shearing device and placed directly into the FRS sample holder that had been preheated to 60 °C. To preserve the microstructure, care was taken to keep the sample above the melting point of the PEO block during the transfer between the shearing and FRS apparatuses. Forced Rayleigh scattering measurements were then performed, at 60 °C, as a function of angle between the shear axis of the sample and the FRS measurement direction, i.e., the grating normal.

Pulsed-Field-Gradient NMR. PFG-NMR was employed to measure self-diffusion of the (unlabeled) OE-6 copolymer, the OE-12 and OE-13 copolymers, and the PEE homopolymer, following standard procedures;[19,20] measurements on PEO homopolymers have been reported previously.[21] The temperature was controlled to within ±0.2 °C. Before beginning each experiment, approximately 20 min was allowed for equilibration at the desired temperature. The stimulated echo three-pulse rf sequence was employed in most of this work. The attenuated echo signal A was recorded at each of six to ten values of the field gradient pulse length, δ. Plots of ln $A(\delta)/A(\delta=0)$ vs $X = \delta^2G^2(\Delta - \delta/3)$ were constructed, and the diffusion coefficient was determined from their slopes. G and Δ, the magnitude and spacing between the gradient pulses, were 180 G/cm (slightly dependent on temperature) and 100 ms, respectively; a steady field gradient of magnitude G_o = 0.7 G/cm was also employed and required the addition of a small correction term to X. Small curvatures in these echo attenuation plots were found to be consistent with the known dispersity of the polymer specimens; larger curvatures were encountered for conditions where the copolymer is known to adopt the cylindrical microstructure. In the latter cases, no detailed interpretation of the echo attenuation in terms of averaged anisotropic diffusion was attempted.

Static Birefringence. Depolarized transmission measurements were carried out using a home-built apparatus consisting of the following optical train: a He−Ne laser (λ_o = 632.8 nm), a pair of crossed polarizers with the temperature-controlled sample holder placed between, and a photodiode detector. The transmitted intensity was measured as a function of temperature. A sample exhibiting birefringence over length scales of micrometers or larger will produce a nonzero signal, indicating the existence of an anisotropic ordered phase, whereas an isotropic phase, either disordered or ordered, will not show a birefringent signal.[22] This approach has been shown to provide an estimate of the grain size in ordered block copolymer melts.[23]

Results

A. Morphological Characterization. Numerous examples show that the dynamic shear moduli, G' and G'', are sensitive to microstructural changes in block copolymer solutions and melts.[24] Rheological measurements, when combined with small-angle scattering techniques, provide an excellent method to locate phase boundaries and to identify the ordered structures present. The temperature dependence of G' for OE-6 during a heating−cooling−heating cycle is shown in Figure 1, as previously reported;[12] illustrations of each morphology are shown as insets. The morphology assignment was based on SAXS measurements, and the phases are labeled L_c, C, and G to indicate crystalline lamellar,

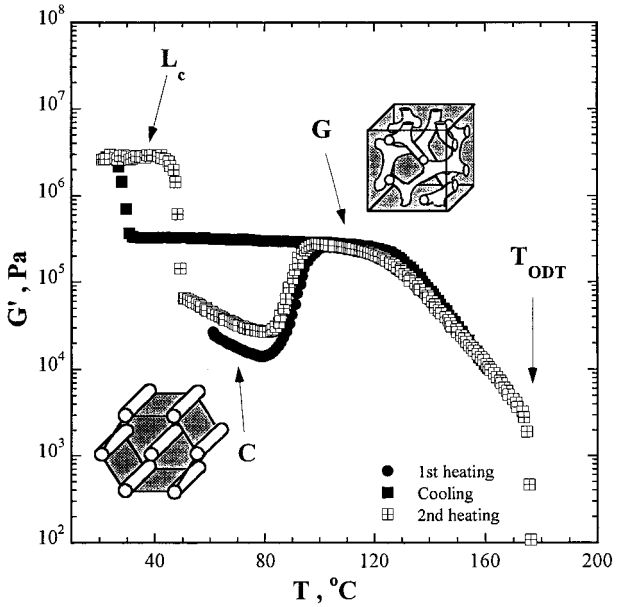

Figure 1. Dynamic elastic modulus measured during heating and cooling at 0.5 rad/s and 1.0 °C/min for molten OE-6. The cylinder and gyroid ($Ia\bar{3}d$) morphologies are illustrated as insets.

hexagonal cylinder, and gyroid phases, respectively. During the first heating, there was a significant rise in modulus at 80 °C that often accompanies an order−order transition into a cubic phase. A softening of the material began at 125 °C and persisted until cooling was initiated at 160 °C. Subsequent cooling showed G' to retrace the heating curve until ca. 100 °C, where the magnitude of G' continues along the plateau indicative of the G phase, suggesting that the C → G transition is not readily reversible in this system. The G phase persisted under cooling until PEO crystallization intervened, forming the L_c phase, which destroyed the cubic symmetry. Heating the L_c phase to 45 °C causes it to melt and form C, as observed during the first heating. Increasing temperature further through the C → G transition causes G' to rise and plateau and ultimately soften until the material disorders. The location of the order−disorder transition was established as 175 ± 2 °C, where G' drops by more than 1 order of magnitude over a 2 °C interval. SAXS data taken at 60 °C are shown in Figure 2a (after heating from the crystalline state) and Figure 2b (after cooling from 120 °C). The triangle indicators on these plots designate the allowed reflections for hexagonal cylinders and the $Ia\bar{3}d$ space group, respectively. The indexing of higher order reflections (shown as insets multiplied by a factor of 10) clearly supports hexagonal cylinders and $Ia\bar{3}d$ as the phases for the conditions in Figure 2a,b, respectively. Annealing experiments in the C phase show it to be a long-lived metastable intermediate. Cylinders were observed to persist for at least 24 h (no transition to G observed) at 60 °C, whereas at 80 °C, the C phase persists for only 15 min before transforming to G. Similar experiments in the G phase at 60 °C showed no transitions to C. The kinetics of order−order transitions in these systems are not fully understood at this time, but recent studies suggest that the matching of principal spacings between morphologies, chain dynamics, and fluctuations can all play significant roles.[13,25]

B. Homopolymer and Disordered Copolymer Self-Diffusion. Self-diffusion coefficients of PEO and

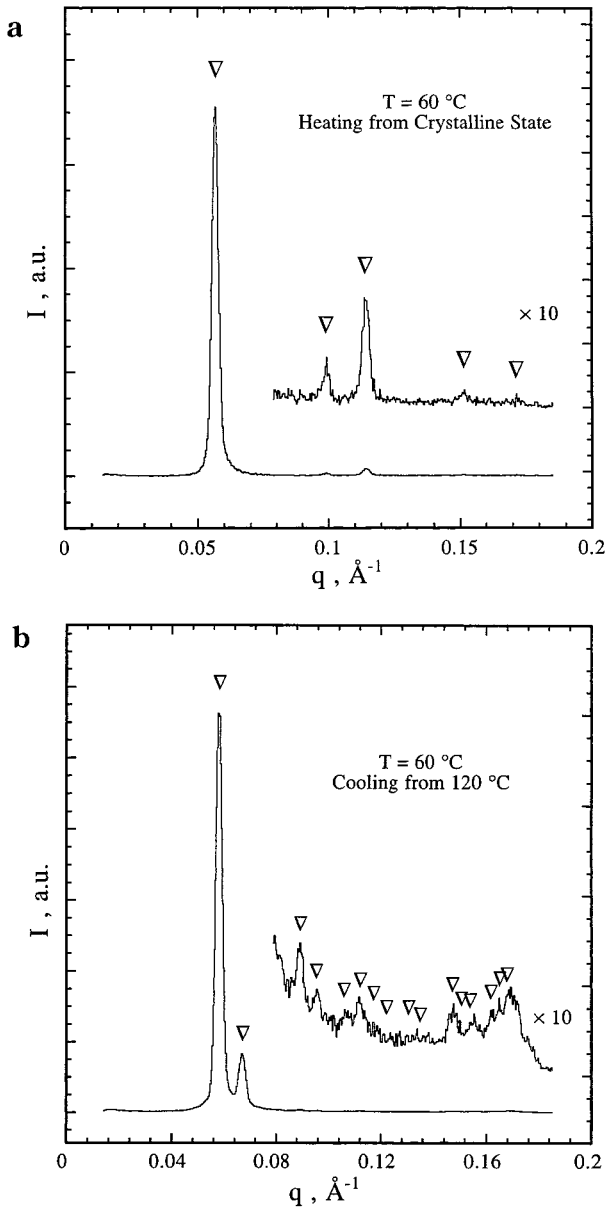

Figure 2. Radially averaged SAXS intensity as a function of scattering wave vector, q, for OE-6 at 60 °C (a) after heating from the crystalline state and (b) after cooling from 120 °C. Triangles indicate positions of allowed reflections for (a) the hexagonal phase, i.e., $\sqrt{1}$:$\sqrt{3}$:$\sqrt{4}$:$\sqrt{7}$:$\sqrt{9}$, and (b) the $Ia\bar{3}d$ space group, i.e., $\sqrt{6}$:$\sqrt{8}$:$\sqrt{14}$:$\sqrt{16}$:$\sqrt{}$:$\sqrt{22}$:$\sqrt{24}$:$\sqrt{26}$:$\sqrt{30}$:$\sqrt{32}$:$\sqrt{38}$:$\sqrt{40}$:$\sqrt{42}$:$\sqrt{50}$.

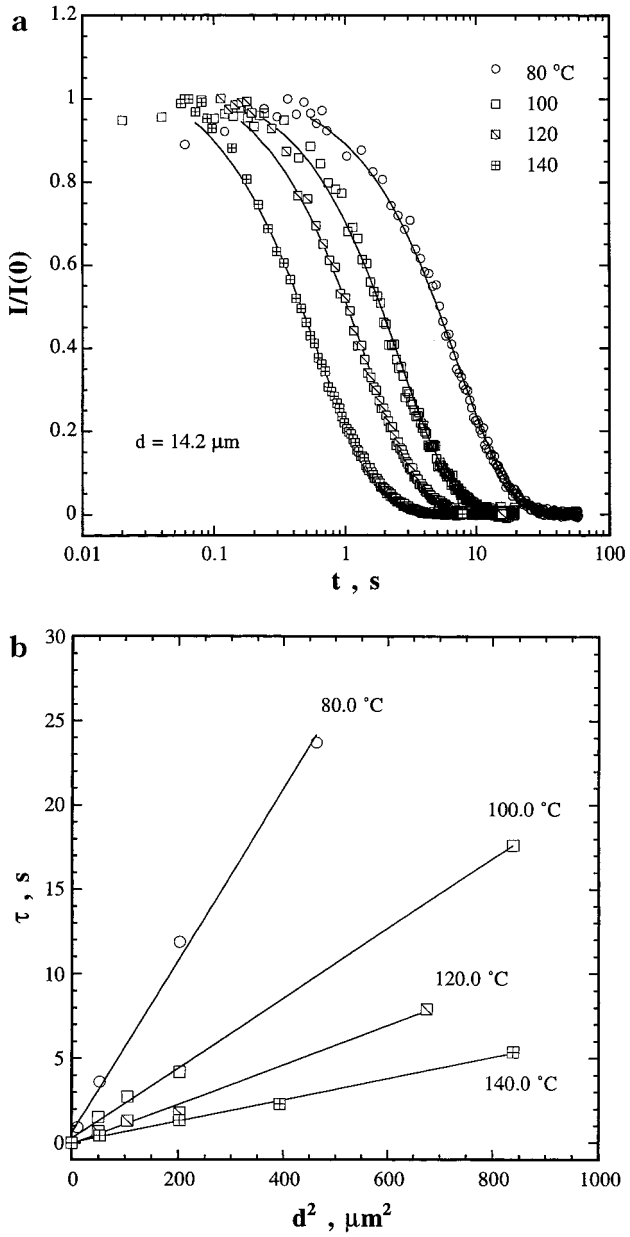

Figure 3. (a) Representative FRS decays taken in the gyroid phase, at the indicated temperatures. The smooth curves through the data are single-exponential fits. (b) Representative plots of decay time versus grating spacing squared, for the same conditions as in (a).

PEE homopolymers were measured by PFG-NMR. The PEO homopolymer diffusion coefficients presented here were reported previously by Cheng et al.[21] The PEO homopolymer molecular weight was given as 1470 g/mol with a polydispersity of 1.05. The results were scaled to the molecular weight of the OE-6 copolymer, assuming the applicability of the Rouse theory expression

$$D = \frac{kT}{N\zeta} \tag{3}$$

where N is the degree of polymerization and ζ is the monomeric friction factor. Use of this relation is reasonable considering the low molecular weights involved, the large distance from the glass transition, and the known entanglement molecular weights ($M_{e,PEO} = 1.7 \times 10^3$ and $M_{e,PEE} = 1.1 \times 10^4$);[15] the same approach was employed for the OE-12 and OE-13 data. However, it is conceivable that OE-6 should be viewed as entangled, given that its total molecular weight is more than twice $M_{e,PEO}$. If one were to use reptation scaling, then the scaled PEO homopolymer and OE-12 and OE-13 data would be reduced by an additional factor of order 2. These homopolymer and disordered copolymer mobilities serve as an informative reference with which to compare the copolymer data.

C. Self-Diffusion in the Gyroid Phase. Typical FRS decays observed in the G phase are shown in Figure 3a, for four temperatures at a grating spacing of 14.2 μm. After an incoherent baseline subtraction, the data were normalized to unit amplitude and placed on a logarithmic time scale. The smooth curves through the data represent single-exponential fits according to eq 1. As is standard practice, the first 5−15% of the points are not included in the fits, because this portion

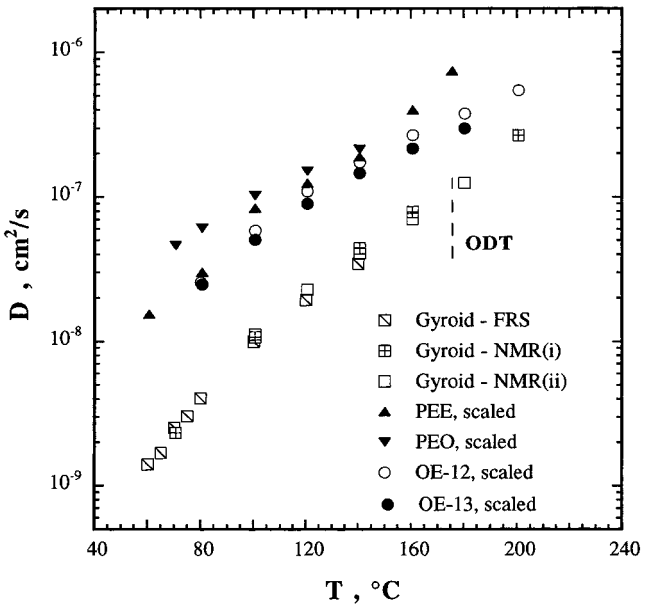

Figure 4. Diffusivity of the OE-6 copolymer measured by NMR and FRS in the gyroid phase and the disordered phase. Also shown are the diffusivities of the constituent homopolymers, PEO and PEE, and the disordered OE-12 and OE-13 copolymers, after Rouse scaling to the molecular weight of OE-6.

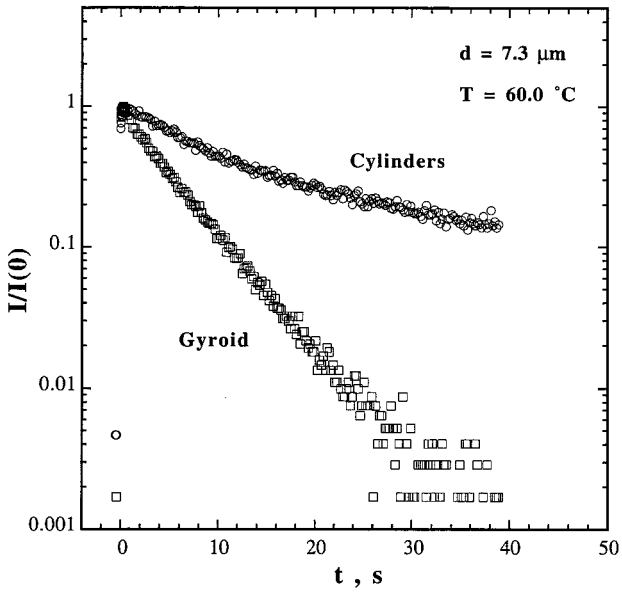

Figure 5. Comparison of typical FRS decays between the gyroid and cylinder morphologies, taken under identical conditions, $d = 7.3\ \mu$m and $T = 60$ °C.

of the FRS signal may contain contributions from dye rotation and thermal relaxation, as well as the convolution of the writing pulse with the sample response function. Clearly, the fits are very good, indicating that one relaxation mode is sufficient to describe the long-time decay kinetics, as one might anticipate on the basis of the cubic symmetry. Moreover, at each temperature, we examined the FRS decay times as a function of grating spacing. A representative plot containing τ versus d^2 for these four temperatures is shown in Figure 3b. In all cases, a linear relationship (with zero intercept) was observed between τ and d^2, confirming the diffusive origin of the relaxation process. The diffusion coefficient can then be determined from the slope, i.e., $D = d^2/4\pi^2\tau$. Additionally, D was calculated from the reciprocal plots ($1/\tau$ vs $1/d^2$), with equivalent results. The reported diffusivity is the arithmetic mean of these two values. The uncertainties in D (<10%) are smaller than the data points, hence the error bars have been omitted from plots containing diffusivities.

The self-diffusion of OE-6 was measured with FRS over the temperature range from 60 to 140 °C, and the results are shown in Figure 4. The FRS sample contained 0.82 wt % labeled chains. This concentration is low compared to typical tracer polymer concentrations used in FRS experiments. However, care needs to be taken when making FRS measurements on labeled block copolymers to ensure that the dye plays no special role in polymer diffusion, such as dye−dye interactions causing association of labeled chain ends. To this end, we also employed PFG-NMR with unlabeled samples to confirm the FRS self-diffusion measurements and to extend the temperature range into the disordered state. Within experimental uncertainty, the diffusion coefficients determined from each technique are identical, which demonstrates that the dye is not causing anomalous behavior in this system. Furthermore, the NMR measurements were repeated approximately one year later (data set ii in Figure 4) and were equivalent. Two interesting features emerge from these data. First, there is no apparent change in the temperature dependence of D upon traversing the ODT. Second, the scaled homopolymer and disordered copolymer diffusivities (also shown in Figure 4) are significantly greater than those of OE-6. Possible implications of these features will be discussed subsequently.

D. Self-Diffusion in Quenched Cylinders. The self-diffusivity of OE-6 in the C phase was measured at 60 °C, after heating the sample from the L_c phase. The hysteresis thus permitted measurements at the same temperature, but in different morphologies. After incoherent baselines were subtracted and normalization to unit amplitudes, representative FRS results for both the G and C phases at 60 °C, and a grating spacing of 7.3 μm, are presented in Figure 5. The intensity is plotted logarithmically to facilitate the determination of single exponential behavior. Linearity of the decay from the G phase clearly indicates single-exponential behavior, which was seen at all temperatures, as discussed above. However, the diffusion in the C phase is different for two reasons. First, the FRS decay is obviously much slower, indicating a smaller diffusion coefficient in C. Second, the decay is clearly not linear, implying a non-single-exponential relaxation. Therefore, the FRS decays arising from the C morphology were fit to eq 2, which produced two time constants, τ_{fast} and τ_{slow}. These are plotted as a function of d^2 in Figure 6. (The range of d^2 is necessarily smaller than in Figure 3b, due to the reduced mobility and to the metastability of the C phase). Each decay constant exhibits a linear dependence on d^2 with zero intercept, indicating that the chains are diffusing at two distinct rates; however, it is also possible that there are two distributions of decay rates, rather than two single exponentials. This non-single-exponential behavior implies that (i) the "grain" size of the polycrystalline material is comparable to, or even greater than, the grating spacing and (ii) the anisotropy in diffusivity (D_{par} vs D_{perp}) is substantial.[3,4,8,9,21] In the case of OE-6, we are unable to visualize the cylinder grain size by TEM because once the copolymer is cooled (even very rapidly) to below the T_m of PEO, the cylinder morphology is lost, and the L_c structure forms. However, we were able to estimate the

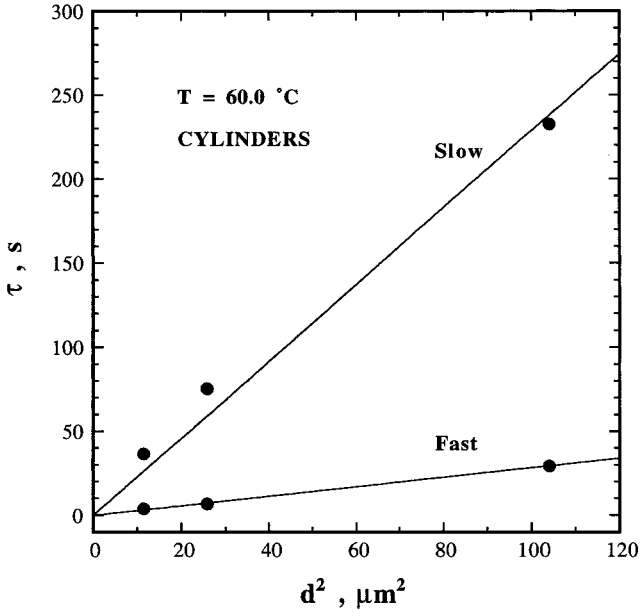

Figure 6. Plot of decay time versus grating spacing squared, for the fast and slow modes of the quenched cylinder phase at 60 °C.

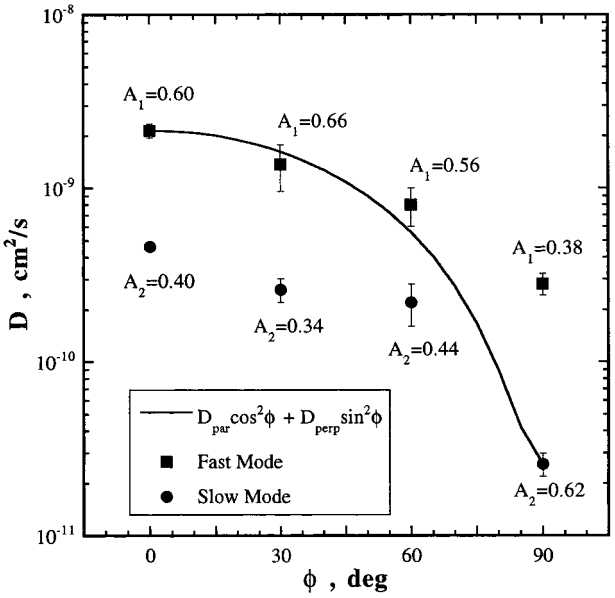

Figure 7. Diffusivity of OE-6 as a function of rotation angle, in the shear-aligned cylinder sample, at 60 °C. The smooth curve indicates the expected projections of D_{par} and D_{perp}. The amplitudes of the modes (according to eq 2) are indicated on the plot.

cylinder grain size to be roughly 4 μm, using static birefringence measurements, by following the approach developed by Balsara and co-workers[23] combined with theoretical predictions for birefringence from Lodge and Fredrickson.[26] Thus the grain size is comparable to the FRS grating spacing and can explain the presence of double exponential decays observed in a quenched sample, as reported previously by Ehlich et al. in a lamellar PS−PI copolymer.[3,4] The faster mode presumably reflects motion primarily along cylinders that have a distribution of orientations about the grating normal, whereas the slower mode involves motion from cylinder to cylinder, and along cylinders lying nearly perpendicular to the grating normal. Consequently, we expect the fast mode diffusivity to be less than D_{par}, and the slow mode diffusivity to be greater than D_{perp}.

E. Self-Diffusion in Shear-Aligned Cylinders. FRS measurements were carried out on a sample that had been subjected to an oscillatory shear field under the conditions described in the Experimental Section. We were unsuccessful in characterizing the degree of alignment with SAXS or TEM, since the long-range order of the microstructure is not preserved upon cooling into the crystalline lamellar phase. However, we can offer indirect evidence for alignment: rheological measurements were performed to observe the response in the dynamic moduli, G' and G'', in situ, after the same shearing conditions had been employed. Both G' and G'' decreased monotonically during the shearing process and reached plateaus that were a factor of 3 less than the initial magnitude. Subsequent frequency sweeps on the shear-aligned sample exhibited moduli that were ca. 4 times smaller than the moduli in the isotropic (unsheared) case. The reduction in moduli that accompanied the shearing is, while not definitive, strong evidence for alignment of the cylinders along the shear direction.[18,27] Furthermore, SANS measurements on a related PEO−PEE sample did indicate orientation of cylindrical domains.[28]

After cessation of the shear alignment, the sample was transferred to the FRS sample holder, and measurements of the self-diffusivity as a function of the angle (ϕ) of the shear direction relative to the FRS measurement axis were carried out. These results are presented in Figure 7. The FRS signals were well described by eq 2. At all values of ϕ, the resulting time constants were linear with d^2, confirming diffusive behavior. As the material has a preferred orientation, we attribute the faster mode at $\phi = 0°$ to D_{par}, or motion along the cylinders, and the slower mode at $\phi = 90°$ to D_{perp}, motion across the cylinders. The second mode we attribute to diffusion in regions of imperfect alignment, which should exhibit a mean diffusivity intermediate between D_{par} and D_{perp}. The curve in Figure 7 represents

$$D = D_{par} \cos^2 \phi + D_{perp} \sin^2 \phi \qquad (4)$$

the expected dependence on ϕ if the sample were perfectly oriented. The points close to the curve contributed ca. 60% of the diffracted amplitude for all four values of ϕ; the actual values of A_1 and A_2 from eq 2 are shown on the plot. The agreement of eq 4 with the faster modes at 30° and 60° supports the interpretation that we indeed measured D_{par} and D_{perp} and that there was a significant degree of alignment. Furthermore, the weaker mode gives an approximately orientation-independent diffusivity, intermediate between D_{par} and D_{perp}, which is consistent with its assignment to regions of imperfect alignment. The resulting ratio between D_{par}/D_{perp} is 83, which is significantly larger than any previously reported anisotropy in block copolymer diffusion.

Discussion

To facilitate the discussion of the above results, the diffusivities obtained at 60 °C in the several morphological states are listed in Table 1. There are four aspects to these results that we will consider: (i) the relative values in Table 1, from a qualitative perspective; (ii) the ratio of D_{par} to D_{perp} in the aligned cylinders; (iii) the ratio of D in the gyroid to D_{par} in the cylinders;

Table 1. Diffusivities at 60 °C

morphology	10^{10} D, cm^2/s
gyroid	14.1
quenched cylinders, fast mode	8.4
quenched cylinders, slow mode	0.96
aligned cylinders, parallel	21.5
aligned cylinders, perpendicular	0.26
aligned cylinders, "defect" mode	2−4

(iv) the copolymer mobilities in comparison to those of the constituent homopolymers and disordered copolymers.

It is reasonable that D_{par} is the largest mobility measured, because for unentangled chains one anticipates that motion along an interface can take place without additional mixing of the blocks, whereas there will be an enthalpic penalty for pulling a block out of a cylinder and transporting it across the majority phase.[29−31] Similarly, one anticipates that D_{perp} will reflect the slowest mode of motion available. This argument also incorporates the plausible, but untested, assumption that mobility through defective regions in the morphology occurs at an intermediate rate. All of the data in Table 1 are consistent with this picture. The minor mode in the aligned state, attributed to diffusion in defective regions in an otherwise reasonably well-aligned sample, gives a mobility sensibly intermediate between D_{par} and D_{perp}. Furthermore, it lies between D_{fast} and D_{slow} in the quenched cylinder sample. As discussed above, we attribute D_{fast} and D_{slow} to a distribution of randomly oriented cylinder grains, with a typical grain size, or "orientational persistence length" of the cylinders, comparable to the meaurement distance. The large difference between D_{par} and D_{perp} suggests that the chains in the quenched sample move a distance d primarily along the cylinder axes, and the resulting distribution of mobilities reflects the distribution of projections of cylinder axes along the grating normal. Finally, the gyroid can, to a first approximation, be considered as a network of cylindrical struts where the mobility along a strut is identical to D_{par}. Consequently, D in the gyroid phase should be lower than D_{par}, by a factor that can be interpreted as the tortuosity of the network. The tortuosity factor from Table 1 is thus about 1.5.

As noted above, the measured anisotropy, $D_{par}/D_{perp} \approx 80$, is the largest yet reported for block copolymer diffusion. Furthermore, this value is likely to be a lower bound to the true anisotropy, due to the inevitable contribution of defects to the measurements even in the well-aligned state. This anisotropy could involve at least three factors: the thermodynamic barrier to pulling the PEO block through the PEE-rich domain; a different mechanism of motion for D_{perp} versus D_{par}; a difference in monomeric friction factors for PEO diffusing in PEE-rich regions, compared to within the PEO domains, and vice versa. It is impossible at this time to resolve these three possibilities, but it is possible to argue that the first factor could be sufficient to explain the measured anisotropy. The barrier to motion should scale as $f\chi N$, which is the enthalpic price for placing the PEO block in a pure PEE domain. Thus,

$$D_{perp} = D_o \exp[-\alpha f \chi N] \qquad (5)$$

where D_o is the bare diffusivity (the mobility in the absence of any thermodynamic interaction) and α is a parameter of order unity. Previous measurements in lamellar PEP−PEE samples suggest that $\alpha \approx 0.6$,[7] whereas Yokoyama and Kramer found $\alpha \approx 1.2$ in spherical PS−PVP materials.[32] We may estimate χN at 60 °C to be ca. 20, utilizing the measured ODTs for two symmetric PEO−PEE copolymers[14] and the Leibler result that $(\chi N)_{ODT} = 10.5$.[33] (However, as these low molecular weight copolymers are predicted to be strongly influenced by composition fluctuations,[34] this value for χN represents a lower bound.) If we make the assumption that $D_{par} = D_o$, as is standard for Rouse chains, then eq 5 (with $\alpha = 0.6$) predicts an anisotropy of 150, which is remarkably consistent with the observed value (e.g., only modest adjustments to χN or α would result in perfect agreement). We may conclude, therefore, that the observed anisotropy can be attributed entirely to the thermodynamic penalty for mixing the blocks. It is worth noting, however, that Helfand has considered the possibility that one block traverses the other microdomain either curled up in a ball or hyperstretched, with either conformation reducing the PEO−PEE contacts and thus the enthalpic penalty.[31] In such a case the barrier in eq 5 would have a lower dependence on N and could therefore accommodate a higher value of χN (as anticipated by the fluctuation theory) and still be consistent with the experimental result.

We now consider a direct comparison between D in the gyroid and D_{par} in the cylinders. Rather than attempt a direct calculation of the tortuosity factor for G, we estimate it in two ways. First, close examination of the G structure indicates that, starting from one strut i, a chain would need to travel along a minimum of 5 struts to reach the nearest strut j that is collinear with i. The linear distance from i to j is equivalent to ca. 3.5 struts. Thus, in the time it takes one chain to diffuse 5 strut lengths, it will move a mean square distance $(5/3.5)^2 \approx 2$ times further along a cylinder than through the gyroid. This is reasonably consistent with the experimentally observed ratio of 1.5, particularly given the possibility that the measured D_{par} is lower than the true value. The second approach is to draw on the calculations performed by Anderson and Wennerström.[35] They computed the ratio D_o/D for various surfactant systems in bicontinuous cubic, L_3, and microemulsion phases, where D is the self-diffusion coefficient of either the water, oil, or surfactant, and D_o is the corresponding diffusion coefficient in an isotropic medium. Analytically, they obtained the ratio to be 1.5 for any particle diffusing on a minimal surface exhibiting cubic symmetry. Although their calculations did not include the $Ia\bar{3}d$ space group, in the closely related space group, $Pn\bar{3}m$, they obtained a value of approximately 1.5, which is entirely consistent with our measurements.

The previous discussion outlines an internally consistent interpretation for the copolymer diffusion data. However, one comparison remains, that between OE-6 and the homopolymer and disordered copolymer mobilities. As noted above, D for the homopolymers and the disordered copolymers are significantly greater than D for OE-6, after accounting for differences in molecular weight via the Rouse model; reptation scaling would reduce, but by no means eliminate, the difference. The data for OE-12 and OE-13 agree rather well, indicating that the pendant hydroxyl group on OE-13 (and OE-6) plays no role and that differences in composition are not important. Furthermore, the OE-12 and OE-13 diffusivities are always close to the slower of D_{PEE} and D_{PEO}, suggesting that a linear combination of component

friction factors applies to the copolymer diffusion. Consequently, we can eliminate friction factor effects as the major source of the difference between OE-6 and the other copolymers. For Rouse chains, one expects $D_{par} \approx D_o$, where D_o is the diffusivity of a fully disordered but otherwise equivalent copolymer, i.e., OE-12. However, this is clearly inconsistent with the results. An alternative approach would be to infer that, in fact, $D_{par} < D_o$ and that these low molecular weight copolymers cannot move readily along the interface. It has been demonstrated that highly entangled copolymers cannot diffuse along the interface without mixing of the blocks, thus incurring an enthalpic penalty,[7] but OE-6 can only be weakly entangled at best. Nevertheless, this appears to be the most plausible explanation. If correct, then the observed anisotropy of a factor of 80 would be significantly less than the difference between D_{perp} in the cylinder phase and D_o. This is also consistent with the fact that D for OE-6 is less than that for OE-12 even in the disordered state; the influence of pretransitional composition fluctuations in retarding entangled copolymer diffusion has been both observed experimentally[36,37] and predicted.[38,39] We also note that the recent theoretical approach of Guenza and Schweizer may be promising in this regard.[40] They find that D/D_o can be substantially reduced even above the ODT, with the ratio decreasing smoothly through the ODT, consistent with the experimental observations. However, as their treatment is a liquid state theory, it cannot address the effect of morphology directly, i.e., in terms of D_{par} and D_{perp}.

Summary

The self-diffusion of a PEO−PEE diblock copolymer has been measured by FRS and NMR, in the gyroid ($Ia\bar{3}d$) and cylinder morphologies. Due to morphological hysteresis, it proved possible to measure D in both microphases at the same temperature (60 °C). FRS measurements on shear-oriented cylinders gave two well-resolved diffusion coefficients, one of which was assigned to diffusion within well-aligned regions of the sample, the other to diffusion within imperfectly aligned, or defective, regions. The resulting values for diffusion along (D_{par}) and across (D_{perp}) the cylinders differed by a factor of 80, an anisotropy that is larger than any previously reported for block copolymer diffusion, but one that is in good agreement with the expectation based on an enthalpic penalty for pulling one PEO block out of one cylinder and inserting it into another. Diffusion in a quenched cylindrical sample indicated a distribution of mobilities, which could be reasonably described by the sum of a fast and a slow diffusive process, both of which were sensibly intermediate between D_{par} and D_{perp}. These were attributed to different projections of cylinder axes along the diffusion direction, coupled with an orientational "grain size" comparable to the FRS diffusion distance (a few microns). Diffusion in the gyroid phase was a factor of approximately 1.5 lower than D_{par}, which is consistent with estimates of the tortuosity of the minor component networks; i.e., the chains diffuse along the struts of the bicontinuous morphology at the same rate as they move along the cylinders. Finally, the diffusion in the gyroid phase was measured as a function of temperature, including in the disordered state, and compared to the self-diffusion of the constituent homopolymers and disordered copolymers. The homopolymers and disordered copolymers diffused significantly more rapidly than did the gyroid sample, even in the disordered state and even after accounting for differences in molecular weight. This is tentatively ascribed to the onset of entanglement effects.

Acknowledgment. This work was supported by the National Science Foundation (NSF-DMR-9528481 to T.P.L.) and by the Center for Interfacial Engineering, an NSF-sponsored Engineering Research Center at the University of Minnesota.

References and Notes

(1) Shull, K. R.; Kramer, E. J.; Bates, F. S.; Rosedale, J. H. *Macromolecules* **1991**, *24*, 1383.
(2) Dalvi, M. C.; Lodge, T. P. *Macromolecules* **1993**, *26*, 859.
(3) Ehlich, D.; Takenaka, M.; Okamoto, S.; Hashimoto, T. *Macromolecules* **1993**, *26*, 189.
(4) Ehlich, D.; Takenaka, M.; Hashimoto, T. *Macromolecules* **1993**, *26*, 492.
(5) Eastman, C. E.; Lodge, T. P. *Macromolecules* **1994**, *27*, 5591.
(6) Dalvi, M. C.; Eastman, C. E.; Lodge, T. P. *Phys. Rev. Lett.* **1993**, *71*, 2591.
(7) Lodge, T. P.; Dalvi, M. C. *Phys. Rev. Lett.* **1995**, *75*, 657.
(8) Hamersky, M. W.; Tirrell, M.; Lodge, T. P. *J. Polym. Sci., Polym. Phys. Ed.* **1996**, *34*, 2899.
(9) Hamersky, M. W.; Tirrell, M.; Lodge, T. P. *Langmuir*, submitted.
(10) Fleischer, G.; Fujara, F.; Stühn, B. *Macromolecules* **1993**, *26*, 2340.
(11) Fleischer, G.; Kärger, J.; Stühn, B. *Colloid Polym. Sci.* **1997**, *275*, 807.
(12) Hillmyer, M. A.; Bates, F. S. *Macromol. Symp.* **1997**, *117*, 121.
(13) Hillmyer, M. A.; Bates, F. S.; Almdal, K.; Mortensen, K.; Ryan, A. J.; Fairclough, P. A. *Science* **1996**, *271*, 976.
(14) Hillmyer, M. A.; Bates, F. S. *Macromolecules* **1996**, *29*, 6994.
(15) Fetters, L. J.; Lohse, D. J.; Richter, D.; Witten, T. A.; Zirkel, A. *Macromolecules* **1994**, *27*, 4639.
(16) Faldi, A.; Tirrell, M.; Lodge, T. P. *Macromolecules* **1994**, *27*, 4176.
(17) Huang, W. J.; Frick, T. S.; Landry, M. R.; Lee, J. A.; Lodge, T. P.; Tirrell, M. *AIChE J.* **1987**, *33*, 573.
(18) Koppi, K. A.; Tirrell, M.; Bates, F. S.; Almdal, K.; Mortensen, K. *J. Rheol.* **1994**, *38*, 999.
(19) von Meerwall, E.; Grigsby, J.; Tomich, D.; Van Antwerp, R. *J. Polym. Sci., Polym. Phys. Ed.* **1982**, *20*, 1037.
(20) von Meerwall, E. D.; Burgan, R. D.; Ferguson, R. D. *J. Magn. Reson.* **1979**, *34*, 339.
(21) Cheng, S. Z. D.; Bailey, J. S.; von Meerwall, E. D. *J. Polym. Sci., Polym. Phys. Ed.* **1991**, *29*, 515.
(22) Balsara, N. P.; Perahia, D.; Safinya, C. R.; Tirrell, M.; Lodge, T. P. *Macromolecules* **1992**, *25*, 3896.
(23) Garetz, B. A.; Newstein, M. C.; Dai, H. J.; Jonnalagadda, S. V.; Balsara, N. P. *Macromolecules* **1993**, *26*, 3151.
(24) See, for example: Fredrickson, G. H.; Bates, F. S. *Annu. Rev. Mater. Sci.* **1996**, *26*, 503 and references therein.
(25) Hajduk, D. A.; Takenouchi, H.; Hillmyer, M. A.; Bates, F. S.; Vigild, M. E.; Almdal, K. *Macromolecules* **1997**, *30*, 3788.
(26) Lodge, T. P.; Fredrickson, G. H. *Macromolecules* **1992**, *25*, 5643.
(27) Ryu, C. Y.; Lee, M. S.; Hajduk, D. A.; Lodge, T. P. *J. Polym. Sci., Polym. Phys. Ed.* **1997**, *35*, 2811.
(28) Hillmyer, M. A.; Bates, F. S. Unpublished results.
(29) Barrat, J.-L.; Fredrickson, G. H. *Macromolecules* **1991**, *24*, 6378.
(30) Fredrickson, G. H.; Milner, S. T. *Mater. Res. Soc. Symp. Proc.* **1990**, *177*, 169.
(31) Helfand, E. *Macromolecules* **1992**, *25*, 492.
(32) Yokoyama, H.; Kramer, E. J. *Macromolecules*, submitted.
(33) Leibler, L. *Macromolecules* **1980**, *13*, 1602.
(34) Fredrickson, G. H.; Helfand, E. *J. Chem. Phys.* **1987**, *87*, 697.
(35) Anderson, D. M.; Wennerström, H. *J. Phys. Chem.* **1990**, *94*, 8683.
(36) Dalvi, M. C.; Lodge, T. P. *Macromolecules* **1994**, *27*, 3487.
(37) Kannan, R. M.; Su, J.; Lodge, T. P. *J. Chem. Phys.* **1998**, *108*, 4634.
(38) Tang, H.; Schweizer, K. S. *J. Chem. Phys.* **1995**, *103*, 6296.
(39) Leibig, C. M.; Fredrickson, G. H. *J. Polym. Sci., Polym. Phys. Ed.* **1996**, *34*, 163.
(40) Guenza, M.; Schweizer, K. S. *J. Chem. Phys.* **1998**, *108*, 1271.

MA971476E